Spectrochimica Acta Part A: Molecular and Biomolecular Spectroscopy 208 (2019) 24–31

Contents lists available at ScienceDirect

Spectrochimica Acta Part A: Molecular and Biomolecular Spectroscopy

journal homepage: www.elsevier.com/locate/saa

# Open path incoherent broadband cavity-enhanced measurements of $NO_3$ radical and aerosol extinction in the North China Plain

K. Suhail [a,b], M. George [b,1], S. Chandran [b,c,d], R. Varma [b], D.S. Venables [e], M. Wang [a], J. Chen [a,*]

[a] School of Energy and Power Engineering, University of Shanghai for Science and Technology, Shanghai, China
[b] Department of Physics, National Institute of Technology Calicut, Calicut 673601, Kerala, India
[c] Physics Department & Environmental Research Institute, University College Cork, Cork, Ireland
[d] Optind Solutions Pvt. LTD. Unit 11, Technology Business Incubator, National Institute of Technology Calicut, Calicut 673601, Kerala, India
[e] School of Chemistry & Environmental Research Institute, University College Cork, Cork, Ireland

ARTICLE INFO

*Article history:*
Received 31 May 2018
Received in revised form 31 August 2018
Accepted 11 September 2018
Available online 15 September 2018

*Keywords:*
Open path
Incoherent broadband cavity enhanced absorption spectroscopy
Nitrate radical
Aerosol extinction

ABSTRACT

We describe the observation of the $NO_3$ radical using an incoherent broadband cavity-enhanced absorption spectrometer in an open-path configuration (OP-IBBCEAS) in a polluted summer environment in continental China. The instrument was installed 17 m above the ground at the top of a residential complex near the CAREBeijing–NCP 2014 site in Wangdu, Hebei province, about 200 km southwest of Beijing over the period 28 to 30 June 2014. The separation between the transmitter and receiver components of the instrument was 335 cm and the effective pathlength in clean reference air was ~3.4 km. $NO_3$ was detected above the detection limit on all three nights when the instrument was operational. The maximum mixing ratio measured was ~175 pptv with a detection sensitivity of ~36 pptv for measurements with an average acquisition time of 10 min. While most extractive instruments try to avoid interferences arising from aerosol extinction, the open path configuration has advantages owing to its ability to detect trace gases even in the presence of aerosol loading. Moreover, concurrent retrieval of aerosol optical extinction is possible from analysis of the absorption magnitude of the oxygen B-band at 687 nm. The experimental setup, its calibration, data acquisition, and analysis procedure are discussed, and the results presented here demonstrate the sensitivity and specificity that can be achieved at high spatial and temporal resolution using the novel configuration of IBBCEAS in the open path.



## 1. Introduction

Non-extractive optical sensing of trace gases has been an important methodology in atmospheric sensing, where instruments like active and passive differential optical absorption spectroscopy (DOAS) are prominent techniques [1,2]. Long physical pathlengths are required in DOAS and related methods for sensitive measurements; this optical configuration results in inherently low spatial resolution which may be problematic when gases have strong local sources or sinks [1,2]. For aerosol extinction measurements, shorter single path transmission measurements have been used [3]. However, for highly reactive atmospheric species and those with strong local point sources, high spatial resolution is desirable.

Long effective optical pathlengths can be realized in a compact instrument using optical cavity-based methods like cavity ring-down spectroscopy (CRDS) [4] and cavity-enhanced absorption spectroscopy (CEAS) [5]. Both methods have been extensively used to monitor $NO_3$ and other species with high sensitivity and high temporal and spatial resolution [6–9]. Significant modifications on CEAS have been based on new light sources such as broadband emitters [10], supercontinuum lasers [11], and frequency combs [12–15], the implementation of advanced detection schemes and off-cavity alignment [16–22].

Extractive sampling is the usual approach used with optical cavity methods. However, sampling effects can be problematic because reactive gases may be lost to tubing and sample cell surfaces. These losses must be quantified for accurate concentration retrieval [8,23]. Such sample modification can be avoided by direct, open path probing of the atmosphere.

There have been few field studies using optical cavities in an open-path configuration, that is, where the optical cavity passes through the open atmosphere [24]. In contrast, the open path configuration has been successfully combined with incoherent broadband cavity-enhanced absorption spectroscopy (IBBCEAS) across numerous atmospheric simulation chambers in studies of trace gases and aerosols [25–27]. Combining broadband optical cavity spectroscopy with an open path configuration allows in-situ detection of the target species in the sample. In 2012 Wu et al. reported the IBBCEAS based instrument

* Corresponding author.
*E-mail address:* j.chen@usst.edu.cn (J. Chen).
[1] Present address: Institute of Environmental Physics Bremen, University of Bremen, Bremen, Germany.

https://doi.org/10.1016/j.saa.2018.09.023

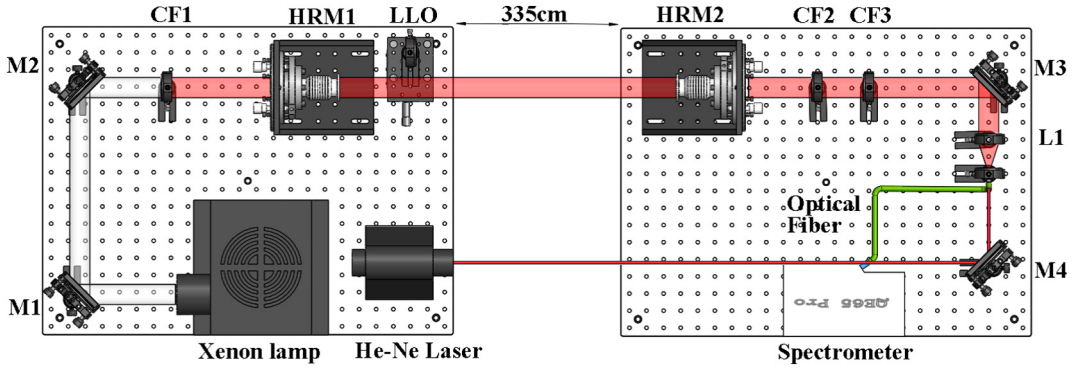


**Fig. 1.** Schematic of the OP-IBBCEAS instrument. M1, M2, M3, and M4 are beam steering mirrors. CF1, CF2, and CF3 are the filters used. HRM1 and HRM2 are high reflectivity dielectric mirrors placed inside holders. L1 is the achromatic doublet used for focusing the beam. LLO is the low-loss optics for calibration.

for simultaneous detection of HONO and $NO_2$ in an open path configuration in a controlled air conditioned laboratory without heavy aerosol loading [28].

In this study, we demonstrate an open path IBBCEAS based instrumentation for simultaneous measurements of the nitrate radical, $NO_3$, and aerosol extinction in a polluted urban location in continental China. $NO_3$ is the dominant nocturnal oxidant and has been a target of interest for several decades [29–34]. It occurs at low mixing ratios in the troposphere (usually at pptv levels) and exhibits strong temporal and spatial variability owing to its high reactivity and short lifetime [25,33,35–37]. $NO_3$ reacts with unsaturated organic species to form compounds such as organic nitrates [38]; its reservoir compound, $N_2O_5$, is an important intermediary in the formation of $HNO_3$ and has been found to produce photolabile chlorine compounds by reacting with particulate chloride [39]. Field measurements of $NO_3$ and $N_2O_5$ have been extensively conducted in both the USA and Europe [9,40,41]. However, observations in China are sparse and mainly limited to Hong Kong, Shanghai, and the North China Plain [42–46] even though satellite observations show that China is a major high NOx region worldwide [46]. In 2016 portable extractive IBBCEAS based instruments were used for field observation of $NO_3$ and $N_2O_5$ in Beijing, China [47].

In this study we present the field deployment of an IBBCEAS system with an open-path configuration where $NO_3$ was observed and aerosol extinction measured simultaneously. Measurements were made at the Wangdu supersite about 200 km southwest of Beijing, China, under conditions of high aerosol loading and high relative humidity. Measurements were part of the CAREBeijing-NCP 2014 Campaign, whose objectives included studying the mechanisms for the production, cycling, and sinks of HOx radicals [48].

## 2. Experimental

### 2.1. Campaign Description

The instrument was located at the Wangdu Supersite, an agricultural location 6 km south east of Wangdu town, Hebei Province (38.7044 N, 115.14 E). The supersite included a wide variety of atmospheric measurement instruments during the one month CAREBeijing-NCP 2014 campaign (7 June–8 July 2014) [48,49]. Wangdu lies in the North China Plain (NCP), a region housing the megacities Beijing and Tianjin, which experiences some of the highest levels of air pollution globally. The NCP is characterized by high NOx air masses that often overlap with high aerosol loadings from both secondary formation and natural sources (e.g. dust from the Gobi Desert in the spring) and serve as an ideal air mass for samples in the study of $NO_X$ chemistry. The site was chosen because it was not directly influenced by anthropogenic emissions or outflow from a megacity, but was expected to observe regionally transported pollution [49]. The surrounding vegetation comprised mainly wheat and willow. The closest major road was 2 km away and there was minimal car and truck traffic in the immediate vicinity [48]. The open path IBBCEAS system was set up on the roof of a building nearby the supersite containers; the instrument was approximately 17 m above ground level. OP-IBBCEAS measurements took place from 28 to 30 June 2014.

### 2.2. Open-Path IBBCEAS

The OP-IBBCEAS instrument is depicted in Fig. 1. A deviation from the conventional CEAS configuration is that the mirrors forming the cavity were placed on separated platforms. One platform housed the transmitter unit comprising the light source (150 W Xe arc lamp), collimating optics, beam steering mirrors (M1, M2), and RG630 long pass optical filter (CF1). The unit also included the entrance cavity mirror. The second platform housed the receiver unit and the second cavity mirror, along with an Andover 650FS80-50 bandpass filter (CF2), Thorlabs 700 nm short pass filter (CF3), focusing optics (mirror M3 and lens L1), and spectrometer (Ocean Optics QEPB0685 TE cooled CCD array). Both the transmitter and receiver units were bolted to heavy metal blocks to ensure mechanical and optical stability. A He-Ne laser housed in the transmitter unit was used to position the

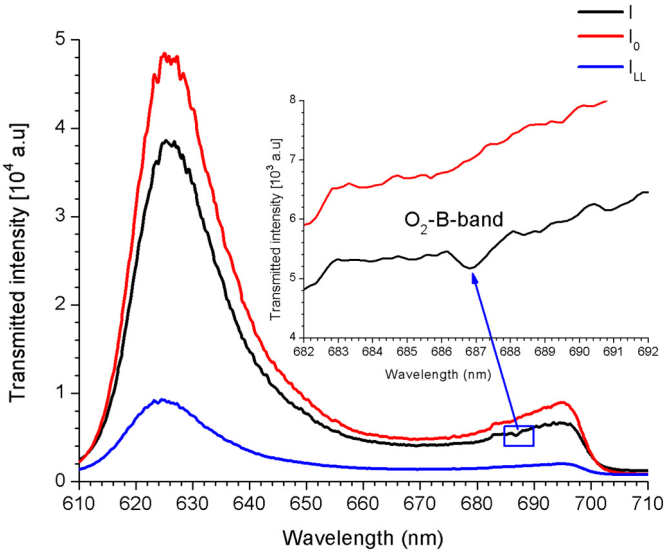


**Fig. 2.** Typical 60 s spectra transmitted through the cavity. The red trace is the reference spectrum ($I_0$, when the cavity was filled with $N_2$), the blue trace ($I_{LL}$) shows the low-loss calibration optic window in the cavity, and the black trace ($I$) is a typical open path spectrum of ambient air. The $O_2$ B-band was only seen in open path spectra and not when the optical cavity was purged with $N_2$. The inset shows a magnified view of the $O_2$ B-band.

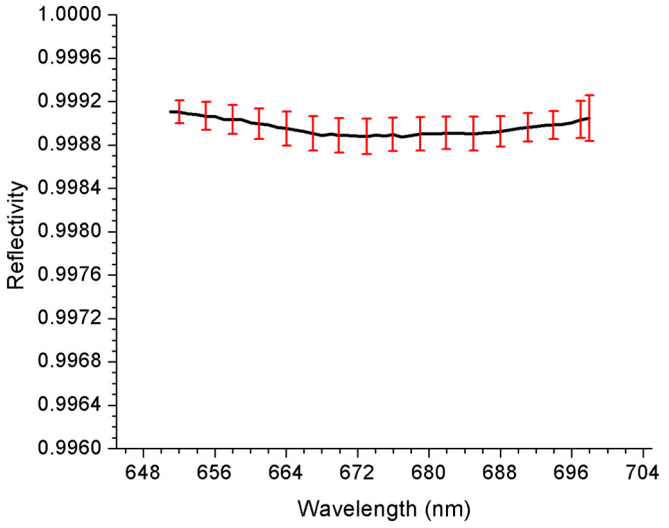


**Fig. 3.** Average mirror reflectivity from all three days of measurements. The error bars represent the standard deviation at corresponding wavelengths with a relative uncertainty of $1.4 \times 10^{-4}$ at 662 nm.

platforms and align the optical cavity. Fine alignment of the system was accomplished by maximizing the cavity transmission spectrum. Stainless-steel pipes of 50 cm length and 8 cm diameter were attached to the transmitter and receiver units (not shown in Fig.1); these pipes enclosed the optical axis and protected the units from rain. The pipes were purged by 5 L $min^{-1}$ of dry nitrogen to protect the cavity mirrors from ambient air and particles. The open air between the two units constituted the sample volume. The optical cavity was 33 cm above the roof surface. The cavity mirrors were 25.4 mm diameter, 5 m radius of curvature (Layertec GmbH). The length of the open path was 335 cm, giving a maximum effective path length of about 7 km based on the manufacturer specified reflectivity of 0.9995 at 660 nm.

The spectrometer wavelength was calibrated using neon atomic emission lines from a neon pen ray lamp. The spectral resolution of the instrument was ~0.47 nm based on the measured width of a He-Ne laser line at 632.8 nm. To measure the reference intensity, $I_0$, a clean, dry atmosphere was introduced in the optical cavity by enclosing it in a 10-cm diameter polyvinyl chloride (PVC) pipe and flushing it with $N_2$. This procedure was carried out every evening before commencing open path measurements. Broadband optical cavity spectra were acquired between 620 nm and 700 nm, which are well within the high mirror reflectivity range specified by the manufacturer.

The calibration of the instrument amounts to determining the effective reflectivity ($R$) of the mirror pair constituting the cavity. We calibrated the instrument using the procedure described in ref. [24], in which a low-loss optical window (with a known pre-calibrated loss spectrum) was inserted into the cavity and its transmission spectrum was recorded. This took place immediately following the $I_0$ reference measurement. Light in the open cavity was absorbed and scattered by atmospheric particles and air molecules once the pipe that introduced nitrogen into the sampling volume was removed. The light intensity $I$ through the open cavity was measured and extinction coefficient spectra were calculated using the IBBCEAS equation: [10,24,50].

$$\alpha(\lambda) = \sum_i \sigma_i(\lambda) \int_0^d n_i(x)dx = \frac{1}{d}\left(\frac{I_0(\lambda)}{I(\lambda)} - 1\right)(1 - R(\lambda)) \quad (1)$$

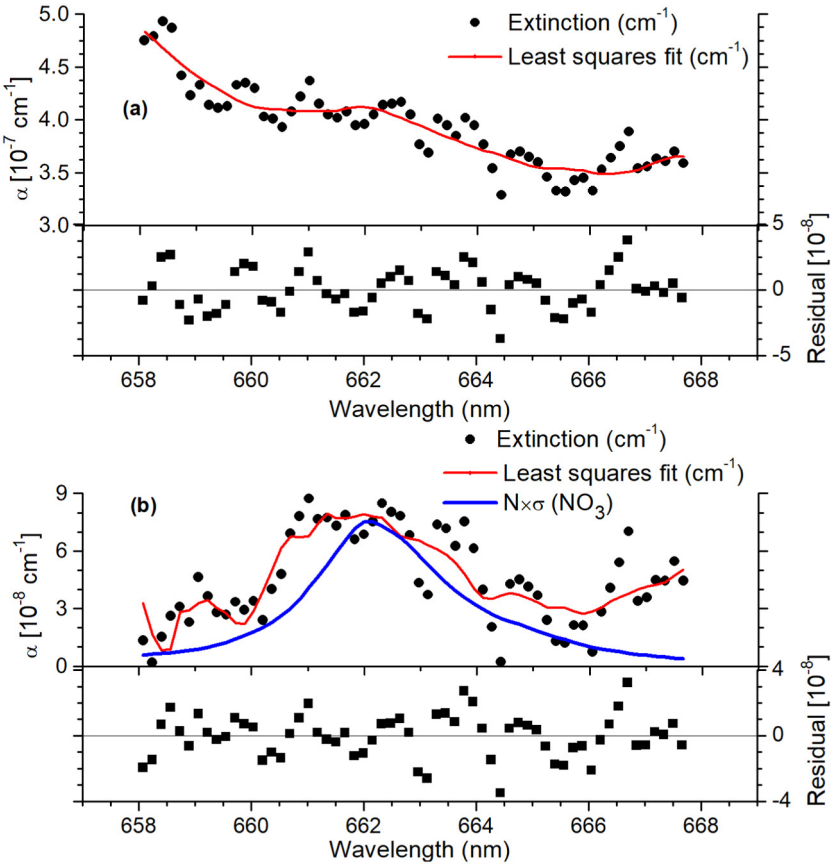


**Fig. 4.** Retrieved extinction spectrum at 04:11 a.m. on 28 June 2014. (a) The measured extinction spectrum (solid circles) in the region 657–669 nm and SVD fit (solid curve) of Eq. (1) to the experimental spectrum with the presence of water vapor. (b) The extinction (solid circles) from (a) after removing the water vapor absorption and polynomial baseline; The blue trace shows the extinction due to $NO_3$ absorption in this spectrum. The lower panel of both (a) and (b) shows the corresponding fit residuals.

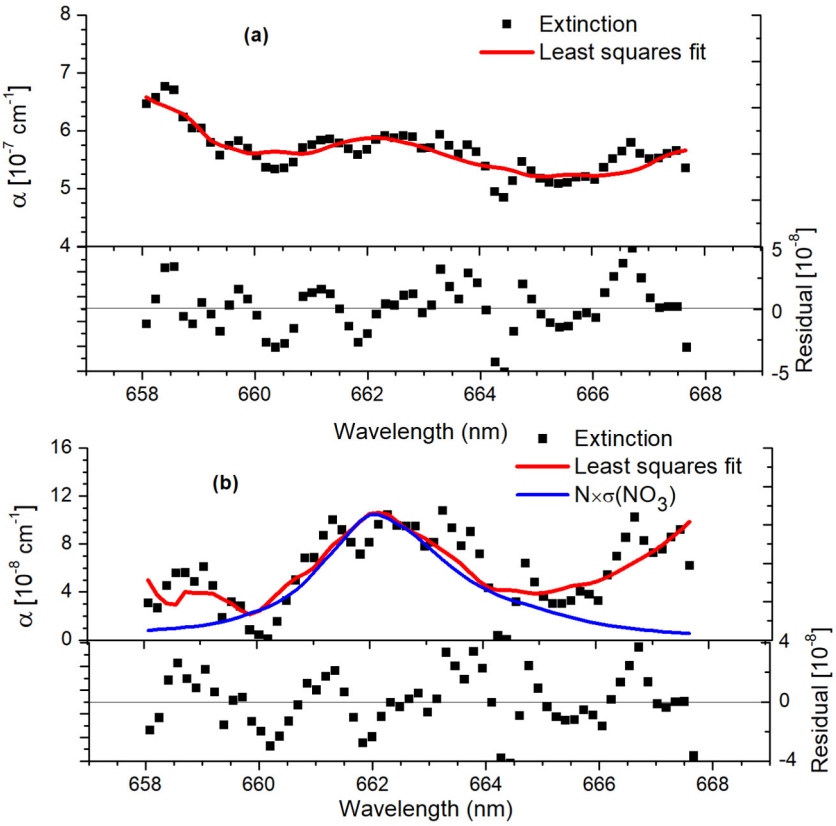


**Fig. 5.** Retrieved extinction spectrum at 02:16 a.m. on 29 June 2014, following the same pattern as in Fig. 4.

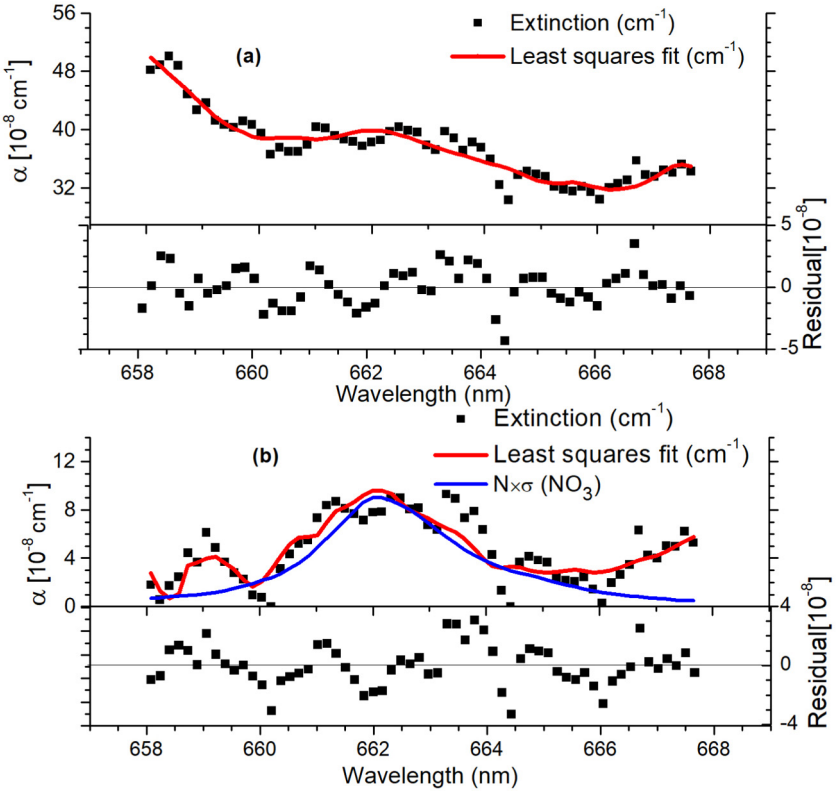


**Fig. 6.** Retrieved extinction spectrum at 04:02 a.m. on 30 June 2014, following the same pattern as in Fig. 4.

where the number of molecules (of an absorbing species) present in the sample of length $d$ is $n$. The $n_i$ and $\sigma_i$ are the number density and absorption cross-section of $i^{th}$ molecule species, $I_0$ is the reference cavity transmission signal (when $N_2$ gas filled the cavity), $I$ is the sample cavity transmission signal and $R$ is the effective mirror reflectivity. Spectra were acquired every 60 s and averaged for 10 min prior to analysis.

A program developed in LabVIEW environment controlled the data collection and spectral analyses were carried out using an embedded MATLAB program. The $NO_3$ concentration was retrieved by fitting each spectrum with cross-sections of $NO_3$, $NO_2$, and water vapor. The literature $NO_3$ cross-section spectrum [51], convolved to the instrument resolution and the 658–668 nm spectral window, was used for retrieving $NO_3$ concentration. Aerosol and other broadband extinction features were accounted for by a polynomial baseline. A singular value decomposition analysis (SVD) based linear least square fit approach [24] was used as fitting routine.

The mirror reflectivity was calibrated by inserting a pre-calibrated low-loss (anti-reflection coated) optic into the cavity after the reference spectrum was recorded and in a stream of $N_2$. Thereafter the pipe enclosing the optical cavity was removed and monitoring of ambient air commenced. Reference, measurement, and calibration intensity spectra are shown in Fig. 2. Also visible in the spectrum is the forbidden B-band of $O_2$ around 687 nm (inset, Fig. 2). Measuring this weak line is an indicator of the instrument's high sensitivity.

The effective reflectivity of the mirror pairs forming the cavity between transmitter and receiver boxes was calculated from spectra transmitted by low-loss optic window. The average effective reflectivity spectrum with standard deviations from all three days of measurements is shown in Fig. 3.

The effective optical path length $d(1-R)^{-1}$ in a clean atmosphere was about 6.5 km with $R \sim 0.9990$ at 660 nm. However, aerosol light scattering greatly reduces this effective path length, which is seen as an increase in the baseline of the extinction spectrum. High aerosol loading thereby limits the sensitivity obtained by the optical cavity in OP configuration.

## 3. Results and Discussion

### 3.1. Analysis of Spectra

Intensity spectra were collected over the three consecutive nights during which the instrument was operational. Typical extinction spectra for each night when measurable $NO_3$ absorption was present are shown in panel (a) of Figs. 4–6. The spectra are dominated by water absorption and aerosol extinction and the $NO_3$ absorption features are not obvious. This is typical for small signal retrievals, for instance in DOAS spectra.

Moderate resolution spectrographs such as ours do not resolve the water absorption lines and give rise to apparent deviations from Beer-Lambert behavior. Previous open-path measurements have observed similar effects arising from water absorption in this spectral region [24,52]. To retrieve accurate $NO_3$ concentrations, absorption by water vapor must therefore be accounted for in the spectral fits. We used the water absorption cross-section spectrum from the HITRAN 2004

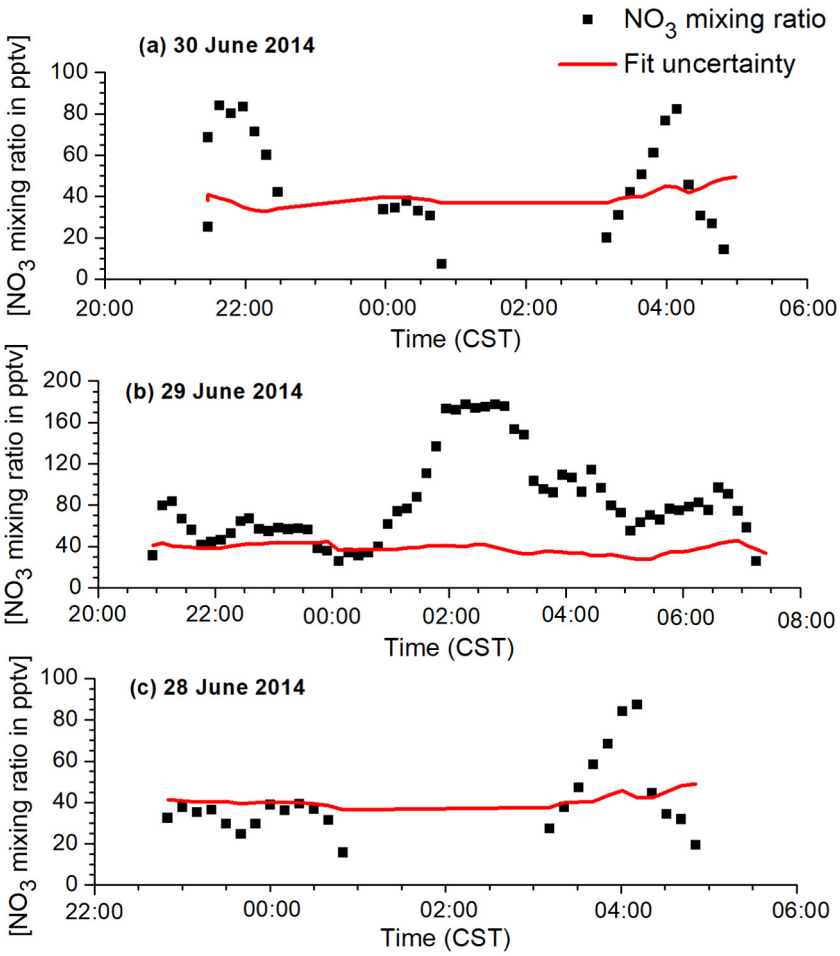


**Fig. 7.** Black trace (solid square) shows the real time $NO_3$ mixing ratio for all three days. The red trace (solid line) shows the estimated fit uncertainty of the measurements. The maximum mixing ratio (~175pptv) for $NO_3$ was recorded on 29 June 2014.

database [53] and convolved it to our instrument resolution. This approach essentially ignores apparent deviations from Beer-Lambert behavior. To study the influence of non-linear water absorption, we used ten different concentration-dependent water absorption cross-sections (synthetically generated and convolved to the instrument resolution) and re-analyzed the one spectrum with high $NO_3$ concentration on each night. These synthetic water cross-sections were generated at high resolution for low to high water concentrations (corresponding to ~2% to ~70% RH range at 23 °C). The spectral fitting (and retrieved $NO_3$ concentrations) did not change appreciably with concentration-dependent water absorption cross sections. We attribute the minor influence of non-linear water absorption to the high aerosol extinction in the polluted Wangdu atmosphere, which reduces the effective optical pathlength and thus the nonlinear effects of stronger absorption lines.

The OP-IBBCEAS extinction spectrum was fitted to the sum of a baseline polynomial of third order as well as number concentrations of water vapor, $NO_3$ and $NO_2$. Representative extinction coefficient spectra corresponding to times when higher $NO_3$ concentration values were retrieved for each night, after removing water absorption and a polynomial baseline are shown in panel (b) in Figs. 4–6. The fit residual below each panel indicates that the water absorption has been largely accounted for.

The fit uncertainty in the retrieved concentrations increased in the presence of high aerosol extinction, which reduced the effective path length and decreased the observed $NO_3$ absorption. The fit uncertainty (taking covariance into account) in the $NO_3$ mixing ratio was typically about 40 pptv during the measurements, which is indicative of the sensitivity of the instrument under the high aerosol loadings present in the North China Plain. Fig. 7 shows the time series of $NO_3$ concentrations retrieved for all three nights.

The errors from the fits indicated a minimum detectable concentration of ~ 40 pptv throughout the operational days in the campaign. On all three nights $NO_3$ was detected at quite high levels with a highest value of about 175 pptv observed at 3 a.m. on 29th of June. The sun rises soon after 4:20 a.m. at this latitude during summer, so measurements made after this time are not as reliable because stray light influenced the spectra. Nevertheless, $NO_3$ concentrations were observed to drop sharply after sunrise on 29 June, as expected from its fast photodissociation in sunlight.

### 3.2. Aerosol Extinction

Aerosol extinction was retrieved based on its effect on the measured $O_2$ B-band absorption in the optical cavity; it was quantified using the formula developed by Varma et al. [24,54]:

$$\varepsilon_B = \alpha_B\left(\frac{I}{\Delta I_A}\right) - \left(\frac{1-R}{d}\right) \quad (2)$$

where $\Delta I_A = I_B - I$. Here $I_B$ is the transmitted intensity when only spectrally broad and unstructured background extinction is present, and $I$ is the transmitted intensity with the presence of both broad background extinction and structured sample absorption. $\alpha_B$ is the oxygen absorption coefficient and $\varepsilon_B$ is the aerosol optical depth or extinction corresponding to the $O_2$ B band wavelength. In the previous studies [24], $\alpha_B$ was calculated using a scaling factor obtained from $I_0$ measurements with dry air in which $O_2$ is a major component. This was not possible in the current case as the $I_0$ was measured with the cavity filled with $N_2$. Instead, we used the scaled value of the average $\alpha_B$ obtained in Varma et al. (2009) [24], as the constant alpha value for $O_2$ absorption; because the number density of oxygen molecules in a real atmosphere is assumed to be constant at ~21% of the total number density of air. The average $\alpha_B$ used in Varma et al. 2009 was ~$5.23 \times 10^{-7}$ $cm^{-1}$ [24].

The spectral resolution of the detection system used in Varma et al. was ~0.6 nm [24]. In the present study the spectral resolution of detection system was ~0.47 nm. The scaling factor for absorption coefficient reported in Varma et al. 2009 [24] to the new resolution of 0.47 nm is same as the ratio of convoluted cross-sections of $O_2$ in corresponding detection resolution (0.47 nm and 0.6 nm) by assuming same number

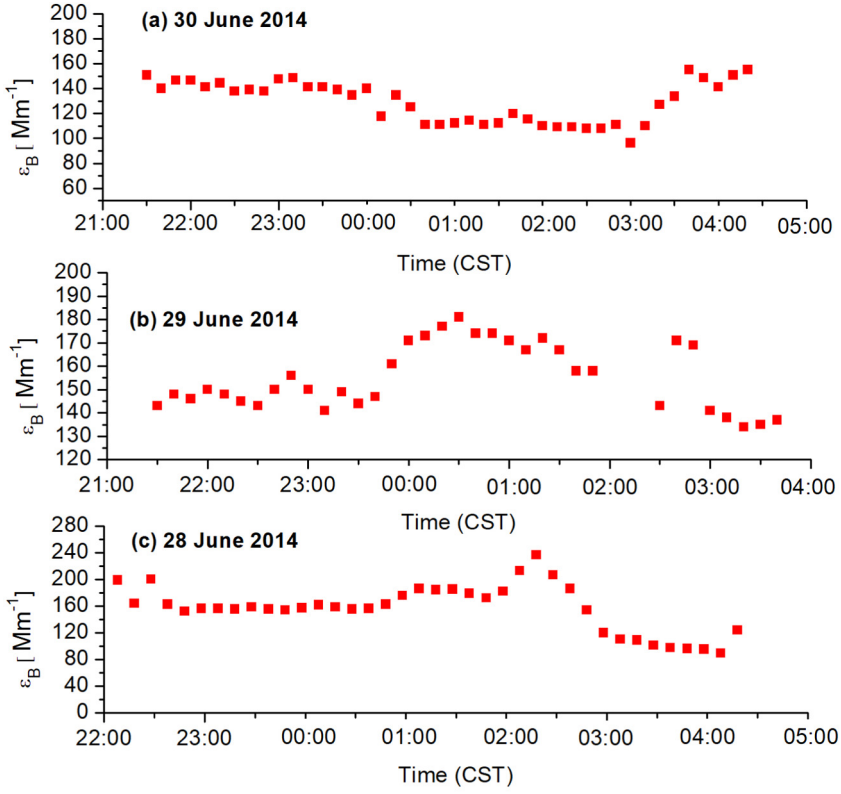


**Fig. 8.** Retrieved aerosol extinction or aerosol optical depth corresponding to the $O_2$—B band wavelength during all the three nights of the $NO_3$ measurements.

density of $O_2$. The scaling factor calculated was ~1.07 and the new $\alpha_B$ generated using this scaling factor was ~$5.6 \times 10^{-7}$ $cm^{-1}$. We used this as our new $\alpha_B$ and retrieved the aerosol extinction following the method reported by Varma et al. (2009). This assumption would at best introduce a multiplicative factor close to unity, but the overall time series of retrieved aerosol extinction would retain the actual trend. The aerosol extinction was retrieved for all three days when $NO_3$ measurements were made and shown in Fig. 8. The aerosol extinction at 687 nm was found to fall in the range of 80–250 $Mm^{-1}$ and is consistent with typical extinctions in this environment [55].

## 4. Conclusions

The OP-IBBCEAS technique that has been reliably used in simulation chamber measurements as well as in extractive mode laboratory monitoring has been successfully applied in real-time in situ monitoring of the tropospheric $NO_3$ during three nights at the Wangdu supersite of the CAREBEIJING-NCP 2014 campaign. The instrument operation was stable for the entire duration of observations and the optical alignment was not affected by the occasional winds or weather. The instrument detected moderately high levels of $NO_3$ on all three nights of operation, with a maximum value of ~175 pptv on June 30th with a corresponding uncertainty of 36 pptv. The retrieved aerosol optical depth was in the range of 80–250 $Mm^{-1}$ at 687 nm when the instrument was not interrupted by rain. This experiment demonstrates the feasibility of the open path IBBCEAS configuration for continuous and long-term observations of trace pollutant $NO_3$ (and other trace gases) with high spatial and temporal resolution.

Potential non-linear absorption by water vapor did not influence the fit results, which likely shows that the instrument sensitivity was limited by the high level of aerosol loading. Under conditions of high atmospheric extinction, whether from high aerosol loading or precipitation, the performance of the open path approach is reduced because the effective optical pathlength is noticeably shorter. Increasing the mirror reflectivity or increasing the mirror separation in the cavity under these conditions would not appreciably increase the system's sensitivity because high atmospheric extinction limits the attainable effective pathlength. While the OP-IBBCEAS approach differs from CRDS in its ability to retrieve aerosol extinction and trace gas concentrations simultaneously, high aerosol loadings reduce the instrument sensitivity to trace gas absorption. We have shown that the OP-IBBCEAS works well in the NCP region under high aerosol loading conditions to monitor $NO_3$ concentration with good sensitivity. This method would generally be more sensitive under cleaner conditions elsewhere.

## Acknowledgements

We gratefully acknowledge the financial support from Science Foundation Ireland, ISCA India Award code: SFI/13/ISCA/2844. R. Varma would like to acknowledge the Department of Science and Technology, Government of India, SERC grant no. LOP/0008/2010 and the Technology Education Quality Improvement Program of the Ministry of Human Resources Development, India, grant number P2/3331/2009. The technical supports by K. Lu and H. Wang during the campaign and the National Science Foundation of China grant number NO. 91544225 are gratefully acknowledged. We are indebted to Prof. A. A. Ruth for providing components and access to experimental facilities in the Laser Spectroscopy Group, University College Cork, Cork, Ireland. The authors also thankful to Dr. S.I. Issac and P. Neeraj for their help and support in data analysis and manuscript preparations.

## References

[1] U. Platt, J. Stutz, Differential Optical Absorption Spectroscopy, Springer, 2008.
[2] J.M. Flaud, C. Camy-Peyret, J.W. Brault, C.P. Rinsland, D. Cariolle, Nighttime and daytime variation of atmospheric NO2 from ground-based infrared measurements, Geophys. Res. Lett. 15 (1988) 261–264.
[3] P.M.S. Chandran, C.P. Krishnakumar, W. Yuenb, M.J. Rood, R. Varma, An open-path laser transmissometer for atmospheric extinction measurements, Am. Inst. Phys. Conf. Proc. 1391 (2011) 288–290.
[4] R. Engeln, Cavity Ring-down Spectroscopy Techniques and Applications, Wiley Publication, 2009.
[5] G. Gagliardi, H.P. Loock, Cavity-enhanced spectroscopy and sensing, Springer Ser. Opt. Sci. 179 (2014).
[6] H.P. Dorn, R.L. Apodaca, S.M. Ball, T. Brauers, S.S. Brown, J.N. Crowley, W.P. Dubé, H. Fuchs, R. Häseler, U. Heitmann, R.L. Jones, A. Kiendler-Scharr, I. Labazan, J.M. Langridge, J. Meinen, T.F. Mentel, U. Platt, D. Pöhler, F. Rohrer, A.A. Ruth, E. Schlosser, G. Schuster, A.J.L. Shillings, W.R. Simpson, J. Thieser, R. Tillmann, R. Varma, D.S. Venables, A. Wahner, Intercomparison of NO3 radical detection instruments in the atmosphere simulation chamber SAPHIR, Atmos. Meas. Tech. 6 (2013) 1111–1140.
[7] S.S. Brown, H. Stark, A.R. Ravishankara, Cavity ring-down spectroscopy for atmospheric trace gas detection: application to the nitrate radical (NO3), Appl. Phys. B Lasers Opt. 75 (2002) 173–182.
[8] W.P. Dubé, S.S. Brown, H.D. Osthoff, M.R. Nunley, S.J. Ciciora, M.W. Paris, R.J. McLaughlin, A. Ravishankara, Aircraft instrument for simultaneous, in situ measurement of NO3 and N2O5 via pulsed cavity ring-down spectroscopy, Rev. Sci. Instrum. 77 (2006), 034101. .
[9] S.S. Brown, W.P. Dubé, H.D. Osthoff, D.E. Wolfe, W.M. Angevine, A.R. Ravishankara, High resolution vertical distributions of NO3 and N2O5 through the nocturnal boundary layer, Atmos. Chem. Phys. 7 (2007) 139–149.
[10] S.E. Fiedler, A. Hese, A.A. Ruth, Incoherent broad- band cavity-enhanced absorption spectroscopy, Chem. Phys. Lett. 371 (2003) 284–294.
[11] J.M. Langridge, T. Laurila, R.S. Watt, R.L. Jones, C.F. Kaminski, J. Hult, Cavity enhanced absorption spectroscopy of multiple trace gas species using a supercontinuum radiation source, Opt. Express 16 (2008) 10178–10188.
[12] M.J. Thorpe, K.D. Moll, R.J. Jones, B. Safdi, J. Ye, Broadband cavity ringdown spectroscopy for sensitive and rapid molecular detection, Science 311 (2006) 1595–1599.
[13] M.J. Thorpe, D. Balslev-Clausen, M.S. Kirchner, J. Ye, Cavity-enhanced optical frequency comb spectroscopy: application to human breath analysis, Opt. Express 16 (2008) 2387–2397.
[14] M.J. Thorpe, J. Ye, Cavity-enhanced direct frequency comb spectroscopy, Appl. Phys. B Lasers Opt. 91 (2008) 397–414.
[15] S. Chandran, S. Mahon, A.A. Ruth, J. Braddell, M.D. Gutiérrez, Cavity-enhanced absorption detection of H2S in the near-infrared using a gain-switched frequency comb laser, Appl. Phys. B Lasers Opt. 124 (2018) 63.
[16] A.A. Ruth, J. Orphal, S.E. Fiedler, Fourier-transform cavity-enhanced absorption spectroscopy using an incoherent broadband light source, Appl. Opt. 46 (2007) 3611–3616.
[17] J. Orphal, A.A. Ruth, High-resolution Fourier-transform cavity-enhanced absorption spectroscopy in the near-infrared using an incoherent broad-band light source, Opt. Express 16 (2008) 19232–19243.
[18] D.M. O'Leary, A.A. Ruth, S. Dixneuf, J. Orphal, R. Varma, The near infrared cavity-enhanced absorption spectrum of methyl cyanide, J. Quant. Spectrosc. Radiat. Transf. 113 (2012) 1138–1147.
[19] S. Chandran, R. Varma, Near infrared cavity enhanced absorption spectra of atmospherically relevant ether-1, 4-Dioxane, Spectrochim. Acta A Mol. Biomol. Spectrosc. 153 (2016) 704–708.
[20] B. Bernhardt, A. Ozawa, P. Jacquet, M. Jacquey, Y. Kobayashi, T. Udem, R. Holzwarth, G. Guelachvili, T.W. Hansch, N. Picque, Cavity-enhanced dual-comb spectroscopy, Nat. Photonics 4 (2010) 55–57.
[21] J.B. Paul, L. Lapson, J.G. Anderson, Ultrasensitive absorption spectroscopy with a high-finesse optical cavity and off-axis alignment, Appl. Opt. 40 (2001) 4904–4910.
[22] S. Chandran, A. Puthukkudy, R. Varma, Dual-wavelength dual-cavity spectrometer for NO2 detection in the presence of aerosol interference, Appl. Phys. B Lasers Opt. 123 (2017) 213.
[23] H. Fuchs, W.P. Dubé, S.J. Ciciora, S.S. Brown, Determination of Inlet transmission and conversion efficiencies for in situ measurements of the nocturnal nitrogen oxides, NO3, N2O5 and NO2, via pulsed cavity ring-down spectroscopy, Anal. Chem. 80 (2008) 6010–6017.
[24] R.M. Varma, D.S. Venables, A.A. Ruth, U. Heitmann, E. Schlosser, S. Dixneuf, Long optical cavities for open-path monitoring of atmospheric trace gases and aerosol extinction, Appl. Opt. 48 (2009) (B159-B71).
[25] H.P. Dorn, R.L. Apodaca, S.M. Ball, T. Brauers, S.S. Brown, J.N. Crowley, W.P. Dubé, H. Fuchs, R. Häseler, U. Heitmann, R.L. Jones, A. Kiendler-Scharr, I. Labazan, J.M. Langridge, J. Meinen, T.F. Mentel, U. Platt, D. Pöhler, F. Rohrer, A.A. Ruth, E. Schlosser, G. Schuster, A.J.L. Shillings, W.R. Simpson, J. Thieser, R. Tillmann, R. Varma, D.S. Venables, A. Wahner, Intercomparison of NO3 radical detection instruments in the atmosphere simulation chamber SAPHIR, Atmos. Meas. Tech. 6 (2013) 1111–1140.
[26] D.S. Venables, T. Gherman, J. Orphal, J.C. Wenger, A.A. Ruth, High sensitivity in situ monitoring of NO3 in an atmospheric simulation chamber using incoherent broadband cavity-enhanced absorption spectroscopy, Environ. Sci. Technol. 40 (2006) 6758–6763.
[27] J. Chen, J.C. Wenger, D.S. Venables, Near-ultraviolet absorption cross sections of nitrophenols and their potential influence on tropospheric oxidation capacity, J. Phys. Chem. A 115 (2011) 12235–12242.
[28] T. Wu, W. Chen, E. Fertein, F. Cazier, D. Dewaele, X. Gao, Development of an open-path incoherent broadband cavity-enhanced spectroscopy based instrument for simultaneous measurement of HONO and NO2 in ambient air, Appl. Phys. B Lasers Opt. 106 (2012) 501–509.
[29] B.J. Allan, N. Carslaw, H. Coe, R.A. Burgess, J.M.C. Plane, Observations of the nitrate radical in the marine boundary layer, J. Atmos. Chem. 33 (1999) 129–154.

[30] U. Platt, G. Lebras, G. Poulet, J.P. Burrows, G. Moortgat, Peroxy radicals from night-time reaction of N03 with organic compounds, Nature 348 (1990) 147–149.
[31] U. Platt, B. Alicke, R. Dubois, A. Geyer, A. Hofzumahaus, F. Holland, M. Martinez, D. Mihelcic, T. Klüpfel, B. Lohrmann, W. Pätz, D. Perner, F. Rohrer, J. Schäfer, J. Stutz, Free radicals and fast photochemistry during BERLIOZ, J. Atmos. Chem. 42 (2002) 359–394.
[32] A. Geyer, B. Alicke, D. Mihelcic, J. Stutz, U. Platt, Comparison of tropospheric NO3 radical measurements by differential optical absorption spectroscopy and matrix isolation electron spin resonance, J. Geophys. Res. Atmos. 104 (1999) 26097–26105.
[33] A. Geyer, B. Alicke, S. Konrad, T. Schmitz, J. Stutz, U. Platt, Chemistry and oxidation capacity of the nitrate radical in the continental boundary layer near Berlin, J. Geophys. Res. Atmos. 106 (2001) 8013–8025.
[34] A. Geyer, B. Alicke, R. Ackermann, M. Martinez, H. Harder, W. Brune, P. di Carlo, E. Williams, T. Jobson, S. Hall, R. Shetter, J. Stutz, Direct observations of daytime NO3: Implications for urban boundary layer chemistry, J. Geophys. Res. Atmos. 108 (2003) 4368.
[35] R. McLaren, R.A. Salmon, J. Liggio, K.L. Hayden, K.G. Anlauf, W.R. Leaitch, Nighttime chemistry at a rural site in the Lower Fraser Valley, Atmos. Environ. 38 (2004) 5837–5848.
[36] J.M.C. Plane, C.F. Nien, Differential optical absorption spectrometer for measuring atmospheric trace gases, Rev. Sci. Instrum. 63 (1992) 1867–1875.
[37] N. Carslaw, L.J. Carpenter, J.M.C. Plane, B.J. Allan, R.A. Burgess, K.C. Clemitshaw, H. Coe, S.A. Penkett, Simultaneous observations of nitrate and peroxy radicals in the marine boundary layer, J. Geophys. Res. Atmos. 102 (1997) 18917–18933.
[38] B.J. Finlayson-Pitss, J.N. Pitts, Chemistry of the Upper and Lower Atmosphere: Theory, Experiments, and Applications, Academic Press, San Diego, 2000.
[39] J.A. Thornton, J.P. Kercher, T.P. Riedel, N.L. Wagner, J. Cozic, J.S. Holloway, W.P. Dubé, G.M. Wolfe, P.K. Quinn, A.M. Middlebrook, B. Alexander, S.S. Brown, A large atomic chlorine source inferred from mid-continental reactive nitrogen chemistry, Nature 464 (2010) 271–274.
[40] J.N. Crowley, G. Schuster, N. Pouvesle, U. Parchatka, H. Fischer, B. Bonn, H. Bingemer, J. Lelieveld, Nocturnal nitrogen oxides at a rural mountain-site in south-western Germany, Atmos. Chem. Phys. 10 (2010) 2795–2812.
[41] A.K. Benton, J.M. Langridge, S.M. Ball, W.J. Bloss, M. Dall'Osto, E. Nemitz, R.M. Harrison, R.L. Jones, Night-time chemistry above London: measurements of NO3 and N2O5 from the BT Tower, Atmos. Chem. Phys. 10 (2010) 9781–9795.
[42] T. Wang, Y.J. Tham, L. Xue, Q. Li, Q. Zha, Z. Wang, S.C.N. Poon, W.P. Dubé, D.R. Blake, P.K.K. Louie, C.W.Y. Luk, W. Tsui, S.S. Brown, Observations of nitryl chloride and modeling its source and effect on ozone in the planetary boundary layer of southern China, J. Geophys. Res. Atmos. 121 (2016) 2476–2489.
[43] S.S. Brown, W.P. Dubé, Y.J. Tham, Q. Zha, L. Xue, S. Poon, Z. Wang, D.R. Blake, W. Tsui, D.D. Parrish, T. Wang, Nighttime chemistry at a high altitude site above Hong Kong, J. Geophys. Res. Atmos. 121 (2016) 2457–2475.
[44] S. Wang, C. Shi, B. Zhou, H. Zhao, Z. Wang, S. Yang, L. Chen, Observation of NO3 radicals over Shanghai, China, Atmos. Environ. 70 (2013) 401–409.
[45] Y.J. Tham, Z. Wang, Q. Li, H. Yun, W. Wang, X. Wang, L. Xue, K. Lu, N. Ma, B. Bohn, X. Li, S. Kecorius, J. Größ, M. Shao, A. Wiedensohler, Y. Zhang, T. Wang, Significant concentrations of nitryl chloride sustained in the morning: investigations of the causes and impacts on ozone production in a polluted region of northern China, Atmos. Chem. Phys. 16 (2016) 14959–14977.
[46] A. Richter, J. Burrows, H. Nüss, C. Granier, U. Niemeier, Increase in tropospheric nitrogen dioxide over China observed from space, Nature 437 (2005) 129.
[47] H. Wang, J. Chen, K. Lu, Development of a portable cavity-enhanced absorption spectrometer for the measurement of ambient NO3 and N2O5: experimental setup, lab characterizations, and field applications in a polluted urban environment, Atmos. Meas. Tech. 10 (2017) 1465–1479.
[48] Z. Tan, H. Fuchs, K. Lu, A. Hofzumahaus, B. Bohn, S. Broch, H. Dong, S. Gomm, R. Häseler, L. He, F. Holland, X. Li, Y. Liu, S. Lu, F. Rohrer, M. Shao, B. Wang, M. Wang, Y. Wu, L. Zeng, Y. Zhang, A. Wahner, Y. Zhang, Radical chemistry at a rural site (Wangdu) in the North China Plain: observation and model calculations of OH, HO2 and RO2 radicals, Atmos. Chem. Phys. 17 (2017) 663–690.
[49] H. Fuchs, Z. Tan, K. Lu, B. Bohn, S. Broch, S.S. Brown, H. Dong, S. Gomm, R. Häseler, L. He, A. Hofzumahaus, F. Holland, X. Li, Y. Liu, S. Lu, K.E. Min, F. Rohrer, M. Shao, B. Wang, M. Wang, Y. Wu, L. Zeng, Y. Zhang, A. Wahner, Y. Zhang, OH reactivity at a rural site (Wangdu) in the North China Plain: contributions from OH reactants and experimental OH budget, Atmos. Chem. Phys. 17 (2017) 645–661.
[50] D.S. Venables, T. Gherman, J. Orphal, J.C. Wenger, A.A. Ruth, High sensitivity in situ monitoring of NO3 in an atmospheric simulation chamber using incoherent broadband cavity-enhanced absorption spectroscopy, Environ. Sci. Technol. 40 (21) (2006) 6758–6763.
[51] R.J. Yokelson, J.B. Burkholder, R.W. Fox, R.K. Talukdar, A.R. Ravishankara, Temperature dependence of the NO3 absorption spectrum, J. Phys. Chem. 98 (1994) 13144–13150.
[52] M. Bitter, S.M. Ball, I.M. Povey, R.L. Jones, A broadband cavity ringdown spectrometer for in-situ measurements of atmospheric trace gases, Atmos. Chem. Phys. 5 (2005) 2547–2560.
[53] L. Rothman, D. Jacquemart, A. Barbe, D. Chris Benner, M. Birk, L. Brown, M. Carleer, C. Chackerian, K. Chance, L. Coudert, et al., The HITRAN 2004 molecular spectroscopic database, J. Quant. Spectrosc. Radiat. Transf. 96 (2005) 139–204.
[54] R. Varma, S.M. Ball, T. Brauers, H.-P. Dorn, U. Heitmann, R.L. Jones, U. Platt, D. Pöhler, A.A. Ruth, A.J.L. Shillings, J. Thieser, A. Wahner, D. Venables, Light extinction by secondary organic aerosol: an intercomparison of three broadband cavity spectrometers, Atmos. Meas. Tech. 6 (2013) 3115–3130.
[55] P. Yan, J. Tang, J. Huang, J.T. Mao, X.J. Zhou, Q. Liu, Z.F. Wang, H.G. Zhou, The measurement of aerosol optical properties at a rural site in Northern China, Atmos. Chem. Phys. 8 (2008) 2229–2242.